Petroleum Science 22 (2025) 384–397

Contents lists available at ScienceDirect

Petroleum Science

journal homepage: www.keaipublishing.com/en/journals/petroleum-science

Original Paper

Mesoporous SiO_2 nanoparticles with low surface energy and multi-level roughness as shale wellbore stabilizers in oil-based drilling fluid

Hong-Yan Du [a, b], Kai-He Lv [a, b, *], Jin-Sheng Sun [a, b, c], Mei-Chun Li [a, b, d], Yuan Geng [c], Xian-Bin Huang [a, b], Hao-Kun Shen [a, b], Muhammad Arqam Khan [a, b, e]

[a] School of Petroleum Engineering, China University of Petroleum, East China, Qingdao, 266580, Shandong, China
[b] Key Laboratory of Unconventional Oil & Gas, Development Ministry of Education, Qingdao, 266580, Shandong, China
[c] CNPC Engineering Technology R&D Company Ltd., Beijing, 102206, China
[d] Co-Innovation Center of Efficient Processing and Utilization of Forest Resources, College of Materials Science and Engineering, Nanjing Forestry University, Nanjing, 210000, Jiangsu, China
[e] Department of Petroleum Engineering, NED University of Engineering & Technology, 395007, Pakistan

ARTICLE INFO

Article history:
Received 5 March 2024
Received in revised form
8 December 2024
Accepted 8 December 2024
Available online 10 December 2024

Edited by Jia-Jia Fei

Keywords:
Fluorosilane
Wettability
Wellbore stability
Drilling engineering
Self-cleaning
Antifouling

ABSTRACT

Oil-based drilling fluids possess excellent properties such as shale inhibition, cuttings suspension, and superior lubrication, making them essential in the development of unconventional oil and gas reservoirs. However, wellbore instability, caused by the invasion of drilling fluids into shale formations, remains a significant challenge for the safe and efficient extraction of shale oil and gas. This work reports the preparation of mesoporous SiO_2 nanoparticles with low surface energy, utilized as multifunctional agents to enhance the performance of oil-based drilling fluids aimed at improving wellbore stability. The results indicate that the coating prepared from these nanoparticles exhibit excellent hydrophobicity and anti-fouling properties, increasing the water contact angle from 32° to 146° and oil contact angle from 24° to 134.8°. Additionally, these nanoparticles exhibit exceptional chemical stability and thermal resistance. Incorporating these nanoparticles into oil-based drilling fluids reduced the surface energy of the mud cake from 34.99 to 8.17 $mJ \cdot m^{-2}$ and increased the roughness of shale from 0.26 to 2.39 μm. These modifications rendered the mud cake and shale surfaces amphiphobic, effectively mitigating capillary infiltration and delaying the long-term strength degradation of shale in oil-based drilling fluids. After 28 days of immersion in oil-based drilling fluid, shale cores treated with MF-SiO_2 exhibited a 30.5% increase in compressive strength compared to untreated cores. Additionally, these nanoparticles demonstrated the ability to penetrate and seal rock pores, reducing the API filtration volume of the drilling fluid from 11.2 to 7.6 mL. This study introduces a novel approach to enhance the development of shale gas and oil resources, offering a promising strategy for wellbore stabilization in oil-based drilling fluid systems.

1. Introduction

Countries all over the world have been paying considerable attention to shale gas, an unconventional oil and gas resource with enormous reserves, in response to the high energy demand brought on by global energy constraints and rapid economic expansion (Zou et al., 2016; Wang, 2018; Bellani et al., 2021). Energy security and the goals of "carbon peaking and carbon neutrality" are greatly impacted by rich shale gas resources, which make it imperative to actively promote its exploration and development (He et al., 2023). Horizontal well drilling technology is widely used in the industrial extraction of shale gas due to its high production capacity and efficiency. However, the technology requires high-performance drilling fluids due to its high drilling complexity, high danger of accidents, and frequent wellbore instability issues in the formation (Huang and Gao, 2022; Lei et al., 2022). Oil-based drilling fluids (ODFs) have superior lubricity and can effectively inhibit the hydration of clay minerals in the formation than water-based drilling fluids (WDFs), and hence can minimize wellbore instability more efficiently (You et al., 2014; Saleh and Ibrahim, 2019; Gao et al., 2021; Karakosta et al., 2021; Du et al., 2022). However, because of

* Corresponding author.
E-mail address: lkh54321@126.com (K.-H. Lv).

https://doi.org/10.1016/j.petsci.2024.12.006

the complicated geological environment of the shale formations, drilling fluids including ODFs invade into the formations through pores and cracks, severely impeding the development of shale gas and potentially leading to severe wellbore instability incidents (Gholami et al., 2018).

The problem of wellbore instability during drilling process is caused by various factors. Shale formations contain abundant amount of hydrophilic clay minerals and oleophilic organic matter, that exhibit amphiphilic features (Siddiqui et al., 2018; Fu et al., 2021). Furthermore, the pores, joints, and fractures in shale formation are well-developed. The pores within are largely micrometer and nanomicron in size. During overbalanced drilling, ODFs invade into the formation through the wellbore fractures and react with the clay mineral and organic matter within, causing it to swell and dissolve. This results in an accumulation of local stress inside the formation and a reduction in the physical strength of wellbore (You et al., 2014). Meanwhile, invasion by fluids in ODF can raise the pore pressure in the formation, increasing the possibility of rock near the wellbore breaking and peeling along the bedding and weak planes, thus causing wellbore instability (Song et al., 2017; Geng et al., 2021; Xie et al., 2023). This indicates that drilling fluid invasion is one of the fundamental driver of wellbore instability in shale gas formation. Therefore, preventing drilling fluid from entering the shale formation during drilling is one of the most crucial measures to maintain wellbore stability.

One of the primary strategies for minimizing drilling fluid intrusion into the formation is to add plugging materials into drilling fluid (Tang et al., 2018; Cheraghian, 2021; Wu et al., 2021; Deng et al., 2022; Yan et al., 2024). Modified asphalt powder and calcium carbonate particles is the most commonly used plugging material (Sun et al., 2021). However, smaller nanoscale pores and fractures are usually impossible for these plugging materials to plug effectively. As nanotechnology develops, nanoparticles are being utilized more and more in the oilfiled and specially in drilling fluids to plug micropores and microcracks in shale formations (Al-Yasiri et al., 2019; Katende et al., 2019; Basfar and Elkatatny, 2023; Cheraghian, 2021; Prajapati et al., 2023; Tahr et al., 2023). At present, commonly used nano plugging materials contain organic, inorganic and composite nano plugging materials. Due to high elasticity and the ability to conform to the pore size of the formation, organic nano plugging materials can produce a dense plugging layer. However, high temperatures can cause the polymer molecular chains to break and the molecular weight to reduce, ultimately leading to a reduction in polymer performance or even failure (Li et al., 2020a; Huang et al., 2022). Therefore, inorganic nano plugging materials, such as SiO_2 nanoparticles and graphene oxide, are used due to their high temperature resistance, environmental friendliness, and wide range of sources (Ma et al., 2019; Wang et al., 2020b; Ali et al., 2022; Geng et al., 2022b; Bardhan et al., 2024). However, due to the high specific surface area, they are prone to agglomeration and are not able to block nanopores in a dispersed state (Assaedi et al., 2016). Composite nano plugging materials combine the advantages of organic and inorganic nano plugging material, but there is still a problem of poor dispersion in ODFs (Mao et al., 2015; Huang et al., 2018; Li et al., 2020b; Meng et al., 2023).

Furthermore, altering the wettability of the shale surface to prevent drilling fluid from invading the formation is another effective strategy to maintain wellbore stability (Ganie et al., 2019). Fluoroalkylsilane (FAS) with hydrophobic fluoroalkyl groups in its molecular tail is a low-surface-energy material, which is widely used for oil-water separation, self-cleaning, and super-biphobic surfaces (Saengkaew et al., 2018; Ou et al., 2020; Parvate et al., 2020; Zha et al., 2024a). And according to the latest literature, FAS showed potential in maintaining wellbore stability. Jiang et al. (2020) developed a hydrophobic low surface free energy nanofluid named SAN as a multifunctional additive for ODF. The SAN was synthesized by the surface sol-gel method of fluorinated group (perfluorooctyl) onto SiO_2 particles. The SAN has been found to have the ability to change the wetting state of shale surface to amphiphobicity, reduce capillary suction of rocks as well as reduce the filtration volume of ODFs. Geng et al. (2022a) used Pickering emulsion polymerization technology to prepare modified nano-SiO_2. Nano-SiO_2 was used as a solid emulsifier to disperse in styrene monomer droplets, and then micron-sized polystyrene particles embedded in SiO_2 nanoparticles were synthesized to construct micro-nano structures. In this study, nanoparticles were inlaid on the surface of micron particles and grafted low surface energy modifiers on the surface, effectively preventing the invasion of ODFs and thus improving the wellbore stability.

Though it is still in its early stage, research on nanomaterials with unique wettability in maintaining wellbore stability in ODFs has demonstrated good practical potential. The low surface energy surfaces with multilevel roughness play a significant role in enhancing material performance, reducing maintenance costs, improving manufacturing processes, and promoting environmental protection (Tang et al., 2024). According to Wenzel's theory, increasing the roughness of the solid surface can further improve the contact angle of the hydrophobic surface ($\theta > 90°$) (Wang et al., 2022b). Mesoporous SiO_2 with rough surface structure has attracted much attention from researchers. Mesoporous SiO_2 nanospheres are three-dimensional central radial fiber structure with a large specific surface area, which have a higher roughness than the traditional SiO_2 microspheres with smooth surface. Furthermore, abundant Si-OH groups on the surface can introduce special functionalized fluorosilane to the surface of SiO_2 microspheres, thereby giving SiO_2 nanoparticles excellent hydrophobic properties (Xu et al., 2022). Due to the above advantages, mesoporous SiO_2 nanospheres are widely used in various fields such as microfluidic, coating technology and drug delivery (Ou et al., 2020).

Therefore, based on the strategy of constructing low surface energy surface with multilevel roughness (Zha et al., 2024b), combined with physical plugging of rock pores, the mesoporous SiO_2 nanoparticles with low surface energy were prepared. This work first prepared mesoporous SiO_2 (M-SiO_2) nanoparticles through Winsor emulsion system. Then, the surface of M-SiO_2 was modified using 1H,1H,2H,2H-perfluorodecyltrimethoxysilane (FAS-17) to prepare the fluorinated modified M-SiO_2 (MF-SiO_2). The dosage of FAS-17 was optimized to achieve a balance between economy and performance. Subsequently, MF-SiO_2 was coated on the surface of the glass slide to evaluate the wettability, self-cleaning, and chemical stability. Finally, MF-SiO_2 was applied to ODF to evaluate the properties on filtration performance and shale wellbore stability. The results indicate that adding MF-SiO_2 into ODF can effectively reduce the filtration volume of ODF, enhance the quality of mud cake, change the wettability of shale to amphiphobic, and weaken the capillary absorption of shale. All of these effects are crucial for the design of high-performance ODFs and the development of unconventional oil and gas resources. This work is expected to provide a new approach for wellbore strengthening technique for ODFs.

2. Materials and methods

2.1. Materials

Urea (99%), hexadecyl trimethyl ammonium bromide (CTAB, 99%), 1H,1H,2H,2H-perfluorodecyltrimethoxysilane (FAS-17, 98%) were purchased from Aladdin Industrial Co., Ltd. In China. N-butanol (99.5%), cyclohexane (99.7%), tetraethyl orthosilicate

(TEOS, 98%), ammonia (25%), hydrochloric acid (HCl), sodium hydroxide (NaOH), calcium chloride ($CaCl_2$), and sodium chloride (NaCl) were purchased from Shanghai Macklin Biochemical Technology Co., Ltd. Hydrogen peroxide was purchased from China National Pharmaceutical Group Chemical Reagent Co., Ltd. All chemical reagents are used as received and do not require further purification. Deionized water is self-made in the laboratory. Mineral oil was purchased from CNPC Great Wall Drilling Company.

2.2. Preparation of mesoporous SiO_2 nanoparticles

The mesoporous SiO_2 nanoparticles were prepared according to previous literature. First, 1.4 g of urea and 1.2 g of CTAB were added in 40 mL of water and sonicated for 30 min as aqueous phase. Subsequently, 1.0 mL of n-butanol, and 6 mL of TEOS were added in 40 mL of cyclohexane and shear emulsification for 30 min as the oil phase. The oil phase was added gradually to the aqueous phase, sheared for 30 min at a high speed (10000 rpm), and then transferred to a flask with three ports. The flask was then immersed in a hot water bath at 80 °C and stirred with magnetic force for 16 h to obtain mesoporous SiO_2 (M-SiO_2). Finally, M-SiO_2 was collected after calcination at 500 °C for 5 h in air to remove the surfactant. In this paper, four experiments were designed, the experimental conditions remain unchanged, only the volume of n-butanol was changed to 0.25, 0.5, 0.75, and 1.0 mL respectively to regulate the depth and distance of wrinkles on the surface of M-SiO_2 nanoparticles.

2.3. Functional modification of M-SiO_2

Firstly, 4.5 g of M-SiO_2 prepared in Section 2.2 was added into a 500 mL mixture of ethanol and water (volume ratio is 9:1), and treated with an ultrasonic mixer for 30 min to fully disperse. Then the pH was adjusted to 8.0 using ammonia and added 0.5 g of FAS-17 to the suspension. Finally, the suspension was transferred to a three necked flask and reacted at 80 °C for 6 h with stirring to obtain the fluoroalkylsilane modified M-SiO_2 (MF-SiO_2). The preparation schematic diagram of MF-SiO_2 is shown in Fig. 1. The prepared MF-SiO_2 solution was centrifuged at 500 rpm for 2 min to obtain the MF-SiO_2 concentrated solution. The concentration of MF-SiO_2 concentrated solution was 65.2 wt%. The appearance of MF-SiO_2 concentrated solution was shown in Fig. S1. In this paper, the dosage of FAS-17 was adjusted to change the grafting density on the surface of MF-SiO_2. The dosage of FAS-17 used was 0.1, 0.5, 1.0 and 3.0 g respectively, while the dosage of other reagents and experimental conditions remained unchanged (Table S1). For simplicity, the final products were denoted as MF*X*-SiO_2 (*X* represents the amount of FAS-17. For example, MF0.5-SiO_2 means 0.5 g of FAS-17 was used to modified 4.5 g M-SiO_2.).

2.4. Characterization of M-SiO_2/MF-SiO_2

The experimental instruments used in this article are shown in Table 1.

2.5. Preparation of M-SiO_2/MF-SiO_2 coating

First, ethanol was used to dilute MF-SiO_2 concentrate solution to around 25 wt%. The glass slide was submerged entirely in a 25 wt% MF-SiO_2 solution, then was taken out right away. The procedure was repeated three times and the slide was dried at 60 °C for 30 min before being used.

2.6. Contact angle and surface free energy calculation

Contact angle testing is a direct means of evaluating surface wettability. Surface free energy is an indicator that describes the surface properties of solids, which is closely related to the wetting and adhesion properties of materials. The wettability and surface free energy of solid surfaces can be determined by measuring the contact angles of different liquids on their surfaces. The static contact angle (CA) was measured using an optical contact angle measuring instrument (Dataphysics, Germany) at room temperature. During the measurement process, the volume of the droplet is 5 μL. Injection speed is 0.1 μL/s. The sliding angle (SA) is obtained by gradually increasing the tilt angle of sample stage until the liquid start sliding. The increase in angle is 1°, and the residence time is 30 s. If the droplet does not slide within 30 s, the inclination angle is increased of the stage by 1° until the droplet slides, and the current angle is recorded as the sliding angle.

The surface free energy is calculated according the Owens, Wendt, Rabel and Kaelble (OWRK) method (Tan et al., 2017). The formula for calculating surface free energy is given as follows:

$$\gamma_S = \gamma_S^D + \gamma_S^P \tag{1}$$

$$\gamma_L(1+\cos\theta) = 2\left(\gamma_S^D\gamma_L^D\right)^{1/2} + 2\left(\gamma_S^P\gamma_L^P\right)^{1/2} \tag{2}$$

where, γ_S is the surface free energy of solid, γ_S^D is the dispersion force of solid, γ_S^p is the polar force of solid, γ_L is the surface tension of liquid, γ_L^D is the dispersion force of liquid, γ_L^P is the polar force of liquid. In this work, water and toluene were used. The variables of surface tension of water and toluene are shown in Table S2.

2.7. Chemical stability test of MF-SiO_2 coating

The stability of drilling fluid additives during the drilling process is a prerequisite for ensuring safe and efficient drilling. Drilling fluid additives must ensure their resistance to corrosion from various chemical reagents, while ensuring that their performance does not deteriorate in high-temperature environments. To assess chemical stability of MF-SiO_2 coating, the MF-SiO_2 coating prepared in Section 2.5 was soaked in water, mineral oil, 0.1 mol/L HCl, 0.1 mol/L NaOH, 20 wt% $CaCl_2$, and 35 wt% NaCl at 25 and 150 °C for 7 days. The soaked glass slide was then taken out and the contact angle of different liquids on its surface was measured.

2.8. Test of surface adhesion force

The adhesion force between liquid and rocks has a significant impact on wellbore stability. If the adhesion between the drilling fluid and the mud cake on the wellbore is poor, it is not easy for the drilling fluid to form a continuous liquid on the wellbore, thereby reducing its permeability to the formation and contributing to maintain wellbore stability. The adhesion force was tested using a surface/interface tension meter DCAT21 (Dataphysics, Germany). A droplet of ~5 μL was suspended at the end of a stainless-steel circle and fixed to a highly sensitive microelectromechanical balance to measure force changes during the experiment. The solid is fixed to the sample stage horizontally and progressively moved the sample stage to get the solid surface closer to the droplet. The position of a droplet as it comes into contact with a solid surface is recorded as the origin. The sample stage begins to move away from the liquid after advancing by 0.5 mm, until it entirely separates from the solid surface. The movement rate of the sample stage during the entire process is 0.1 mm/s. The schematic diagram of surface adhesion force was shown in Fig. S2.

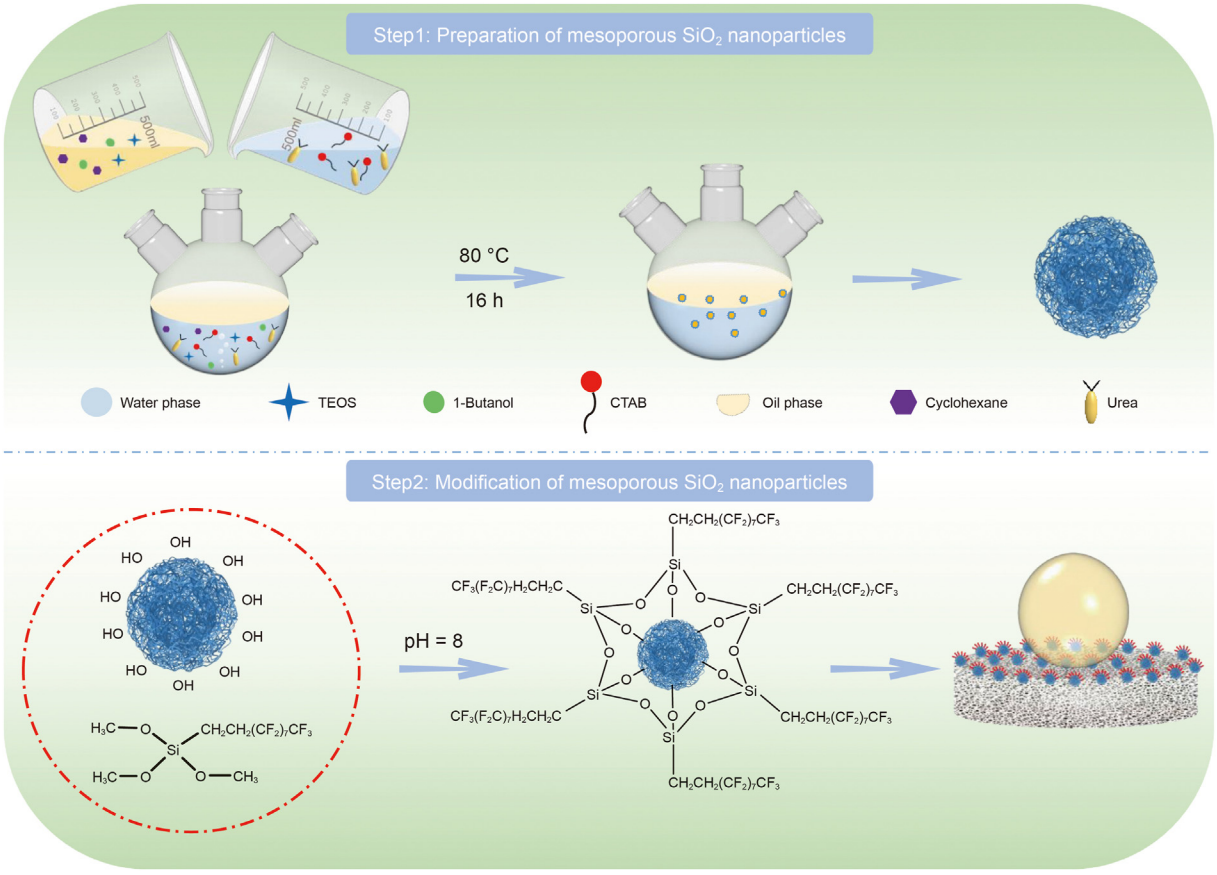

Fig. 1. Schematic diagram of the preparation and modification process of mesoporous SiO_2 nanoparticles.

Table 1
Instruments used for sample characterization.

Instrument	Purpose
FT-IR spectrometer	Used to test the FT-IR spectrum of sample, with a testing frequency range from 4000 to 400 cm^{-1}
Thermogravimetric analyzer	Analyze the thermal performance of the sample under a nitrogen atmosphere, with a test temperature range of 100–1000 °C and a heating rate of 10 °C/min。
Nuclear magnetic resonance spectrometer	Analyze the Si NMR spectrum of the sample at 30 °C and 25° pulses
X-ray photoelectron spectroscopy	Analyze the chemical composition of sample
Scanning electron microscope	Analyze the surface morphology, element types, and content of the sample
Transmission electron microscope	Analyze the microstructure of the sample
Atomic force microscope	Analyze the surface structure and properties of the sample

Table 2
The formulation of WDF.

Material	Dosage	Function
Water	400 mL	Based fluid
Bentonite	12.00 g	Controlling filtration loss
NaOH	0.12 g	Disperse clay, adjust pH
Carboxymethyl cellulose	8.00 g	Controlling filtration loss
KCl	20.00 g	Inhibiting clay expansion
Sulfonated lignite	5.00 g	Controlling filtration loss
Methyl oleate	0.20 g	Lubricant

Table 3
The formulation of oil-based drilling fluid.

Material	Dosage	Function
Mineral oil	320 mL	Based fluid
Lime	5.00 g	Adjust pH
Organic clay	2.00 g	Rheological modifier
Span-80	20.00 g	Emulsifier
Asphalt powder	10.00 g	Controlling filtration loss
Ultrafine calcium carbonate	5.00 g	Controlling filtration loss
20 wt% $CaCl_2$ solution	80 mL	Based fluid

2.9. Preparation of drilling fluids

A typical WDF and ODF was prepared according to Tables 2 and 3. For each material added, a high-speed mixer was used for 20 min. All the additive were provided by Shandong Deshunyuan Petroleum Sci. &Tech. Co. Ltd. The preparation of WDF and ODF samples were obtained from standard API RP 13B-1 (2019) and API RP 13B-2 (2014) respectively.

2.10. Performance evaluation of drilling fluid

Drilling fluid performance testing process according to the American Petroleum Institute standards:

The rheological parameters of the drilling fluid were measured by a six speed rotational rheometer (Fann 35, USA). Viscosity was measured at 600 (θ_{600}) and 300 (θ_{300}) rpm readings. The apparent viscosity (*AV*), plastic viscosity (*PV*), and yield point (*YP*) were calculated using the following relationships:

$$AV = \theta_{600}/2 \text{ (mPa·s)} \tag{3}$$

$$PV = \theta_{600} - \theta_{300} \text{ (mPa·s)} \tag{4}$$

$$YP = (\theta_{300} - PV)/2 \text{ (Pa)} \tag{5}$$

The filtration volume of drilling fluid was measured by a high-temperature and high-pressure filtration instrument (Model GGS42−2, Qingdao Tongchun, China) at a pressure difference of 3.5 MPa and 120 °C.

The emulsion stability (ES) was measured by an electrical stability measurement (Fann 21200, USA) with an electrode distance of 1.55 ± 0.04 mm. The electrode probe was placed in ODF, and the emulsion-breaking voltage was accorded.

2.11. Permeability plugging test

Considering the practical application environment of drilling fluids, ceramic filters with a thickness of 6.35 mm and a diameter of 63.5 mm, a porous medium, were used to simulate formation rocks to evaluate the filtration performance of ODF. The average pore size of ceramic filters is 5 μm. The filtration volume was measured over time at a high-temperature and high-pressure environment (120 °C, 3.5 MPa).

Static filtration is used in the filtration loss tests. The drilling fluid is static in static filtering, while the thickness of filter cake, one of the percolation media (another medium is the filter membrane), is variable and thickens with percolation time. In general, the permeability of filter cake is much lower than that of ceramic filters. If the ratio of filter cake thickness to filter membrane diameter is small enough, it can be assumed that percolation is linear, which avoids the usage of complex percolation modes and is stated by Darcy's law (Du et al., 2022):

$$\frac{dV_f}{dt} = \frac{KAp}{h\mu} \tag{6}$$

where V_f is filtration volume, t is filtration time, K is the permeability of filter cake, A is the filtration area, p is the filtration pressure, h is the thickness of filtrate cake, μ is the filtrate viscosity.

If a certain volume (V_m) of drilling fluid filtrated completely, the following material balance will be achieved:

$$V_m = hA + V_f \tag{7}$$

$$V_s = hAC_c \tag{8}$$

where C_c is the volume fraction of solid in filter cake, V_s is the volume of solid phase in filter cake. The following equation can be obtained from Eqs. (7) and (8):

$$C_m = \frac{V_s}{V_m} = \frac{hAC_c}{hA + V_f} \tag{9}$$

$$h = \frac{V_f}{A\left(\frac{C_c}{C_m} - 1\right)} \tag{10}$$

Thus,

$$\frac{dV_f}{dt} = \frac{KA^2p\left(\frac{C_c}{C_m} - 1\right)}{\mu V_f} \tag{11}$$

The following equation can be obtained by integrating:

$$\frac{V_f^2}{2} = \frac{KA^2p\left(\frac{C_c}{C_m} - 1\right)t}{\mu} \tag{12}$$

$$V_f = A\sqrt{\frac{2Kp\left(\frac{C_c}{C_m} - 1\right)}{\mu}}\sqrt{t} \tag{13}$$

After the filtration experiment, the ODF was replaced with mineral oil, and the filtrate volume was measured at 1.0 MPa after 1 min. The average permeability was calculated accord Eq. (14):

$$K = \frac{Qh\mu}{10tAp} \tag{14}$$

where Q is filtration volume, t is filtration time, K is the permeability of filter cake, A is the filtration area, p is the filtration pressure, h is the thickness of filtrate medium, μ is the filtrate viscosity.

2.12. Capillary imbibition experiment of shale

The core capillary imbibition experiment of shale is one of the methods used in the laboratory to measure the wettability of rocks. On one hand, it allows us to understand the hydrophilic or lipophilic properties of rocks, which is significant for evaluating wellbore stability. On the other hand, core capillary imbibition experiment can also evaluate the effectiveness of different drilling fluid additives in reducing the spontaneous water imbibition capacity of shales. The shale core has been treated with modified nanoparticles before immersion. The processing method is to soak the shale core in MF-SiO_2 solution, and then use the pulling method to adhere the nanoparticles to the surface of the rock core to endow the shale surface with liquid repellent ability. A shale rock core with a length of 25 mm and a diameter of 15 mm was suspended on a highly sensitive electronic balance. The position of the core was adjusted so that the bottom of the core comes in contact with the liquid surface while the changes in core mass over time were monitored.

2.13. Compression strength test

The compressive strength test of shale has a significant impact on wellbore stability. The compressive strength test can evaluate the mechanical strength of the borehole rock and provide a basis for the stability of the borehole. The shale core has been treated with modified nanoparticles before immersion, the processing method is the same as in Section 2.12. The shale rock core with a length of 50 mm and a diameter of 25 mm was dried at 100 °C for 72 h. Afterwards, the shale rock core was soaked for 28 days in water, mineral oil, WDF, and ODF. A microcomputer-controlled rock triaxial test machine (TSE-105D, Wance Technologies Ltd., China) was used to determine the uniaxial compressive strength of shale core following a 72-h drying process in a 100 °C oven. The

displacement loading rate was 2 mm/min, and the loading force was kept constant at 95 kN throughout the testing procedure. The rock core is determined to have fractured when the pressure decreases by 1000 N.

2.14. Surface roughness

One of the methods to improve the contact angle of the hydrophobic surface is to increase the roughness of the solid surface. By measuring and regulating the surface roughness of materials, the hydrophobicity of the surface can be optimized. The surface morphology and roughness of shale was evaluated using a 3D confocal microscopes (DVM6, Leica, Germany). Under laboratory settings (atmospheric pressure, room temperature 25 °C, relative humidity 60%), the samples were viewed under a microscope. Their observations were conducted with an objective (× 100). The light source used is green LED (530 nm), with a bright field objective and confocal mode. All samples were obtained by photographing their surfaces and measuring their topography, size, and roughness.

3. Results and discussion

3.1. Characterization of mesoporous SiO_2 nanoparticles (M-SiO_2)

The SiO_2 nanoparticles with different rough surfaces were prepared as per the synthesis mechanism shown in Fig. 2(a). This reaction system is a special microemulsion system. When TEOS that dissolved in cyclohexane came in contact with water at the oil-water interface, the reaction of hydrolysis and condensation progressed gradually. Specifically, under the action of urea, the resulting mixture consists of negatively charged silicate monomers and oligomers. Influenced by the Coulomb force, negatively charged silicate monomers assemble with the positively charged end of the cationic surfactant. As the reaction progresses, the number of uncharged silicates gradually increases. In order to maintain charge balance, the number of silicates bound to the cationic head of the surfactant increases, resulting in the interface bending towards the aqueous phase. As the curvature of the interface increases, spherical or columnar micelles are formed. The aggregation of these micelles forms repetitive intermediate phases, which can serve as crystalline seeds. With the reaction being continuous, the crystalline seeds grow in the water layer of the double continuous micro emulsion, and the micro emulsion around the nanoparticles is rearranged. Finally, the water layer of the micro emulsion is connected with the ridge of the nanoparticle wrinkles, the oil layer is connected with the valley of the nano particle wrinkles, and the intermediate phase becomes the seed of the nanoparticle, so the overall structure of the synthesized nanoparticle presents a wrinkles shape (Moon and Lee, 2012; Ren et al., 2021). Thereafter, based on the above mechanism, we regulate the wrinkles of M-SiO_2 nanoparticles by adjusting the volume of n-butanol added during the experimental reaction process. The SEM

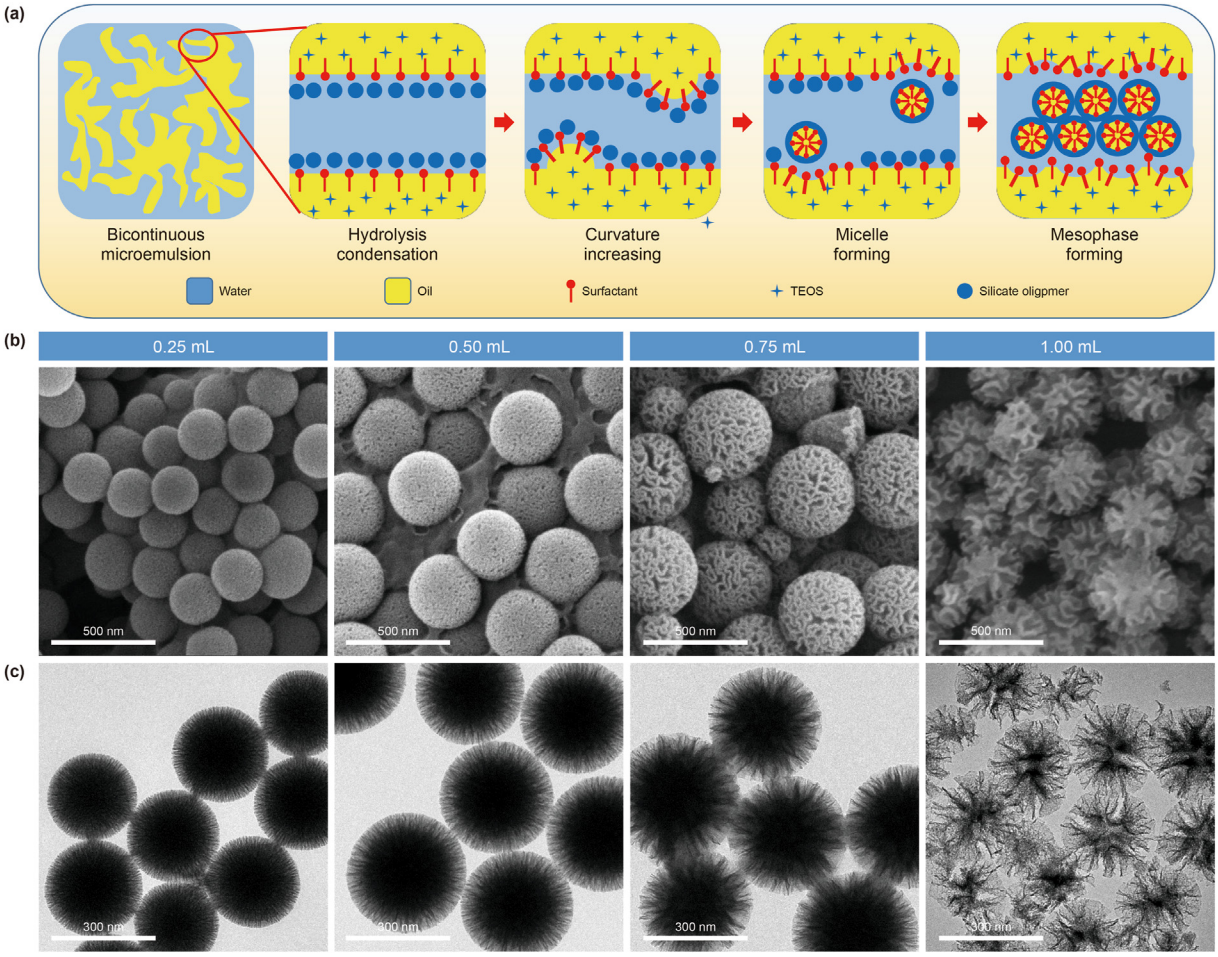

Fig. 2. Synthesis mechanism of mesoporous SiO_2 and surface morphology under different reaction conditions (**a**) Synthesis mechanism of mesoporous SiO_2; (**b**) SEM images; (**c**) TEM images. SEM and TEM images of mesoporous SiO_2 prepared with n-butanol content of 0.25, 0.5, 0.75, and 1.0 mL, respectively.

and TEM images of M-SiO_2 nanoparticles are shown in Fig. 2(b) and (c). The M-SiO_2 nanoparticles are spherical. When the amount of n-butanol added is 0.25 mL, the surface of M-SiO_2 nanoparticles is smooth and the wrinkles distribution is shallow. With the increase of n-butanol content, the wrinkles on the surface of M-SiO_2 nanoparticles extend towards the inside of the particles, and the distance between the wrinkles increases. One of the conditions for achieving a hydrophobic surface is to improve the roughness of the solid surface. However, under the four concentrations of n-butanol, the SiO_2 prepared at a concentration of 1 mL had a higher roughness. Therefore, in the subsequent reaction, the dose of n-butanol was fixed at 1.0 mL.

3.2. Preparation and characteristics of MF-SiO_2 nanoparticles

On the basis of M-SiO_2 nanoparticles, FAS-17 was used to modify M-SiO_2. The coupling agent method is the most commonly utilized method for SiO_2 surface modification. The chemical formula for the silane coupling agent is R-SiX_n. Among them, X is a functional group, such as methoxy group or ethoxy group, which can react with silanol bond via dehydration and condensation; the other group R is an organic reactive group that does not hydrolyze, such as C=C, $-NH_2$, and $-CH_2Cl$, etc., which can easily react with other organic groups and can graft functional materials onto the surface of SiO_2. In this work, the group R is $-CF_2$ and $-CF_3$, which can significantly lower the surface energy of SiO_2.

As shown in Fig. 3(a), after modification, there are still obvious wrinkles on the surface of MF-SiO_2. The TEM image (illustrated in Fig. 3(a)) is consistent with the morphology in Fig. 2(c), which provides a basis for high roughness. The surface morphology of MF-SiO_2 was further characterized by AFM. In a typical AFM height image, black dots display relatively low areas, while highlights display relatively high areas. Fig. S3 shows the representative high-resolution 2D morphology of MF-SiO_2. The surface of MF-SiO_2 is rough, and many wrinkles can be clearly observed from the corresponding 3D oblique images, which improve the surface roughness. The results of surface elements analysis (Fig. 3(b)) show that there are F, C, O and Si elements in MF-SiO_2, and the distribution of F and C elements on the particle surface is uniform, which indicate that FAS-17 is uniformly grafted onto the surface of M-SiO_2. To further demonstrate the successful grafting of FAS-17 onto M-SiO_2 surface, further characterization of MF-SiO_2 nanoparticles were conducted. As shown in Fig. 3(c), the peaks at 786 and 1084 cm^{-1} are caused by the bending vibration of Si—O—Si. After modified with FAS-17, several peaks appeared in the spectrum compared with that of M-SiO_2. Peak at 653 cm^{-1} could be ascribed to the stretching vibration of Si—C, and peaks at 1152 and 1208 cm^{-1} could be ascribed to the stretching vibration of C—F of the $-CF_3$ and $-CF_2$ groups in FAS-17 (Li et al., 2023). As shown in Fig. 3(d), there is one chemical shift of Si—O—Si in the spectrum of M-SiO_2, while a new chemical shift appears in the spectrum of MF-SiO_2, which can be attributed to the Si—C bond. In addition, surface analysis of the MF-SiO_2 was carried out using XPS (Fig. 3(e)). The Si 2p, C 1s, O 1s and F 1s peaks are observed from the spectrum of M-SiO_2 and MF-SiO_2. After normalization, the C 1s and F 1s percentage in MF-SiO_2 is estimated to be 22.46% and 31.78% respectively. Compared to M-SiO_2, the content of C and F elements significantly increased. The Si 2p spectrum (Fig. 3(f)) exhibits two contributions located at 103.9 and 103.4 eV respectively, which can be assigned to Si—O bond and Si—C bond. And the C 1s spectrum (Fig. 3(g)) exhibits five contributions located at 294.2, 291.8, 285.8, 284.9, and 284.2 eV respectively, which can be assigned to CF_3, CF_2, C—H, C—C, and C—Si. All these evidences fully demonstrate the successful modification of MF-SiO_2. Finally, we characterized the thermal performance of MF-SiO_2 modified with different amounts of FAS-17. As can be seen from the TGA curve (Fig. 3(h)), M-SiO_2 has good thermal stability, and the weight loss was less than 10% at 25—1000 °C, which was mainly caused by the evaporation of the adsorbed water on the surface of SiO_2 and the dehydration and condensation of silicon hydroxyl groups in SiO_2. MF-SiO_2 also has good thermal stability, with less than 5% weight loss at 25—300 °C, mainly caused by the evaporation of adsorbed water on the surface. At 300—700 °C, the weight loss gradually increases with the increase of modifier dosage, and the weight loss reaches its peak at 450 °C, and the weight loss was mainly due to the thermal degradation of FAS-17 grafted on the surface of SiO_2. When the temperature was higher than 700 °C, the quality of MF-SiO_2 remains basically stable. The thermal performance test shows that MF-SiO_2 has excellent high temperature resistance, which is favorable for its applications under extreme conditions.

3.3. Surface wettability of MF-SiO_2 coating

In order to evaluate the wettability of MF-SiO_2, MF-SiO_2 was deposited and coated on the surface of a glass slide using the pull-up method (Fig. 4(a)). The most direct means for evaluating the surface wettability are the contact angle and sliding angle (Beitollahpoor et al., 2022). Four liquids, namely water, WDF, mineral oil, and ODF, were tested for their contact angle on the MF-SiO_2 coating (Fig. 4(b)). All liquids have contact angles for MF0-SiO_2 that are less than 35°. When the dosage of FAS-17 was increased to 0.5 g, all four liquids had contact angles more than 120°, and the contact angles of water and WDF even increased to 146° and 144.3° at a dosage of 0.5 g, respectively. There is an insignificant increase in contact angle when FAS-17 dosage is increased further. In addition, as shown in Fig. 4(c), the sliding angle of MF0-SiO_2 is 90° (the liquid did not slide when the glass slide was placed vertically). There is a significant decrease in sliding angles with the dosage of FAS-17 raising. Considering both hydrophobic performance of MF-SiO_2 and cost of FAS-17, we selected the MF0.5-SiO_2 as the optical formula, the particle size distribution of M-SiO_2 and MF-SiO_2 before and after modification was tested, and the particle size distribution of MF-SiO_2 was 270—620 nm (Fig. S4), and evaluated the performance in subsequent experiments. As shown in Fig. 4(d) (up panel), various liquids were dropped onto the surface of the glass slide. Water, mineral oil, WDF and ODF can all wet and spread on the surface of the blank glass slide as blank group. After MF0.5-SiO_2 treatment, the four liquids maintained a clear spherical shape on the surfaces (bottom panel). Subsequently, the anti-fouling tests of MF0.5-SiO_2 coating were conducted. As shown in Fig. 4(e), only ODF had a slight adhesion on the coating surface, whilst the other three samples remained dry and clean. The self-cleaning performance of the coating surface is tested by contaminating surfaces with dust simulation (shale powder). As shown in Fig. 4(f), during the rolling process of liquid droplets from the coating surface, they remained spherical and carried the shale powder away from the coating surface, demonstrating that the excellent capacity for self-cleaning. The excellent non-wetting performance of the coating is attributed to the significant air gap between the mesoporous nanoparticles on the coating surface and the liquid, as well as the reduced adhesion to the surface caused by low surface free energy. Therefore, we measured the adhesion force between different liquids and coating surfaces. As shown in Fig. 4(g), the relationship between adhesion force and distance (the distance between the droplet and the coating surface) included five processes: (1) approaching (from A to B), (2) touching (Point B), (3) droplet compression (from B to C), (4) retracting (from C to D), and (5) detaching (from D to E). At the approaching stage, the interaction forces were always zero prior to making contact with coated surfaces. At the touching stage, the droplets come into contact with the

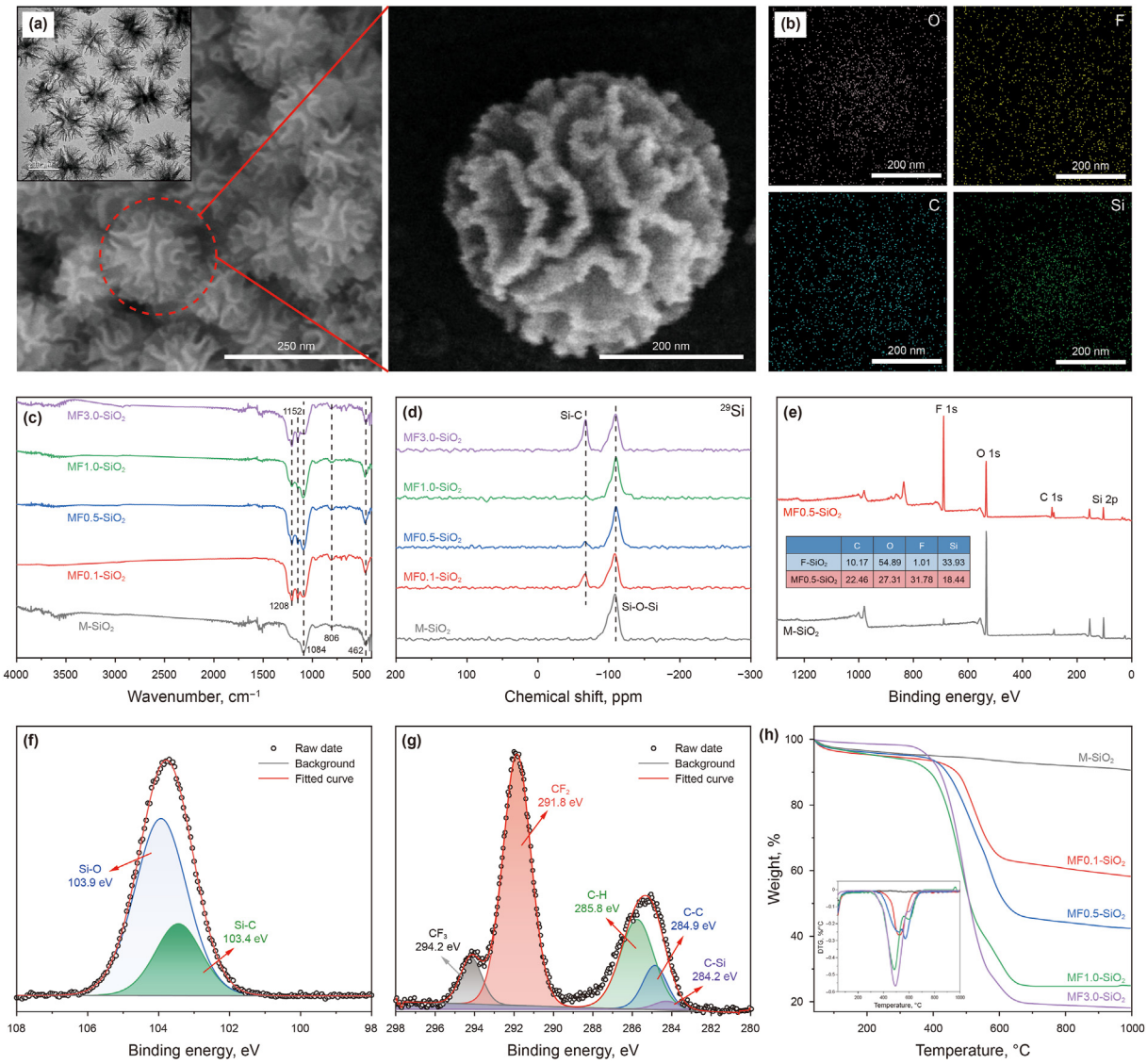

Fig. 3. Characterization of MF-SiO_2 and M-SiO_2: (**a**) SEM and enlarged view images of MF0.5-SiO_2, the illustration is TEM images; (**b**) EDS mapping of C, O, F, and Si elements in MF0.5-SiO_2; (**c**) FT-IR spectra of M-SiO_2 and MF-SiO_2 with various dosages of FAS-17; (**d**) ^{29}Si NMR spectra of M-SiO_2 and MF-SiO_2 modified with different dosages of FAS-17; (**e**) XPS full spectra of M-SiO_2 and MF0.5-SiO_2, the table in the illustration showing the element content; (**f**) the high-resolution XPS spectrum of Si; (**g**) the high-resolution XPS spectrum of C; (**h**) TG curve of M-SiO_2 and MF-SiO_2 modified with various dosages of FAS-17.

surface of the sample as the sample stage continues to rise. At the droplet compression stage, since the droplets remain spherical under the action of surface tension and can not wet the coating surface, the droplets are compressed as the sample stage continue to rise. This upward force results a constant decrease in force. At the retracting stage, the sample stage started to retreat once it reached the set position. The droplet is stretched because of the adhesive force that exists between it and the surface. This stretching produces an upward force, which results in a steady decrease in force. The force peaks at point D, which represents the maximum adhesion force on the surface. On the surface of MF0.5-SiO_2 coating, the adhesion forces of water, WDF, mineral oil, and ODF are 4.1, 30.1, 10.3, and 50.1 μN, respectively. At the detaching stage, the droplets separate from the coated surface as the sample stage retreats, causing a sudden drop in force. The force value did not go back to its initial level because some liquid was stuck to the coated surface. This phenomenon indicates that the cohesion within the droplet is smaller than the adhesion between the droplet and the MF0.5-SiO_2 surface (Wang et al., 2020a, 2022a). Furthermore, during the entire process, adhesion of ODF on the MF0.5-SiO_2 surface is the highest, which accounts for a relatively poor self-cleaning performance of ODF.

High temperature stability has a significant impact on the performance of materials (Yin et al., 2021, 2022a; Li et al., 2024). Considering that the application environment is a high-temperature and high-pressure solution environment, we tested the high-temperature stability of the sample. The surface contact angle was tested after the MF0.5-SiO_2 coatings were heated for 5 h at different temperatures. As shown in Fig. 4(h), it is possible to maintain the contact angle between white oil and water on the sample surface over 120° under 200 °C. However, the contact angle on the sample surface decreases above 300 °C. The contact angle dramatically decreased as the temperature reached 400 °C, indicating serious FAS-17 deterioration. This is consistent with the results of TG (Fig. 3(h)). This result indicates that MF0.5-SiO_2 can maintain long-term lyophobic ability below 200 °C. Coatings

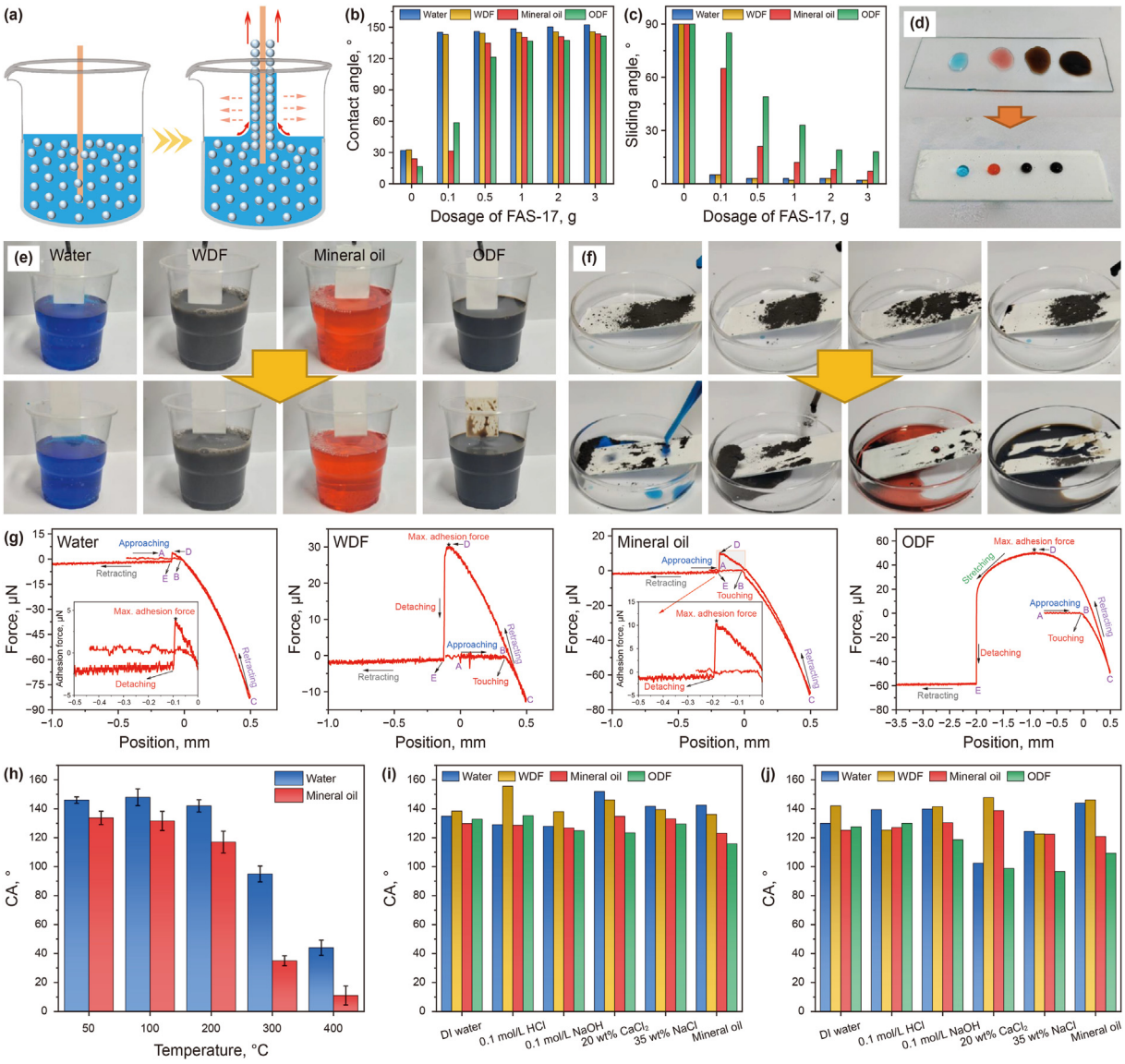

Fig. 4. (**a**) Schematic diagram of MF-SiO_2 coating preparation by pulling method; (**b**) Contact angle and (**c**) sliding angle of MF-SiO_2 coatings prepared with different FAS-17 dosage; (**d**) The spreading state of water, WDF, mineral oil, and ODF on blank glass slides and MF0.5-SiO_2 coating surfaces; (**e**) Anti-fouling test of MF0.5-SiO_2 coating in water, WDF, mineral oil, and ODF; (**f**) Self-cleaning test of the MF-SiO_2 coating when shale powder is placed on the surface and different liquids are dropped; (**g**) Adhesion force test of water, WDF, mineral oil, and ODF on coating surface. (**h**) The contact angle between water and mineral oil on the surface of coatings treated at 50, 100, 200, 300, 400 °C; (**i**) The contact angle of the coating is soaked in acids, alkalis, salts, organic solvents resistance test that aged at 25 °C for 7 days; (**j**) The aged temperature is 150 °C, and other conditions are the same as (**i**).

should not only have a high contact angle in normal environments, but also be stable in harsh environments, especially chemically stable (Yin et al., 2022b, 2022c, 2023a, 2023b; Liu et al., 2023). Additional requirements for application in ODFs include resistance to acid, alkali, inorganic salt, and organic solvents. Therefore, we further evaluated the chemical stability of MF0.5-SiO_2 coating. The MF0.5-SiO_2 coating was immersed in water, 0.1 mol/L HCl, 0.1 mol/L NaOH, 20 wt% $CaCl_2$, 35 wt% NaCl, and mineral oil for several days, and then the contact angles of water, WDF, mineral oil and ODF on their surfaces were tested. It can be seen that the MF0.5-SiO_2 coating can still exhibit good hydrophobicity on its surface after being immersed in the different solutions at room temperature for seven days, with contact angles greater than 120° (Fig. 4(i)). In addition, following a seven-day immersion at 150 °C, the contact angles of the four liquids on the surface of the glass slide slightly decreased, but they remained greater than 90°, suggesting that MF0.5-SiO_2 exhibits excellent chemical stability (Fig. 4(j)).

3.4. Performance evaluation of oil-based drilling fluids

The excellent hydrophobic properties and chemical stability of MF0.5-SiO_2 are prerequisites for its application in ODFs. The effect of MF0.5-SiO_2 on drilling fluid performance requires a further investigation. Drilling safety greatly depends on the rheological and filtration properties of the drilling fluid. In addition, for ODF, the emulsion stability is of critical importance. The drilling fluid additives should not have negative impacts on the performance of the drilling fluid (Rafieefar et al., 2021). The value of emulsion stability (ES) for the basic ODF is 615 V. After the addition of 3% MF0.5-SiO_2 concentrate, the ES value rose to 798 V (Table 4). In addition, the apparent viscosity (*AV*), plastic viscosity (*PV*), and yield point (*YP*) of basic ODF slightly increased, and the filtration volume slightly decreased following the addition of 3% MF-SiO_2. It demonstrates that adding MF-SiO_2 can enhance the emulsion stability while also somewhat increasing the capability to move rock and lowering the

Table 4
The effect of MF0.5-SiO_2 on the emulsion stability, rheology and filtration volume of ODF.

Sample	*ES*, V	*AV*, mPa·s	*PV*, mPa·s	*YP*, Pa	*YP*/*PV*	*FL*, mL
Basic ODF	615	17.0	14.0	3.0	0.21	11.2
Basic ODF +1% MF0.5-SiO_2	746	17.5	13.0	4.5	0.35	8.2
Basic ODF +3%MF0.5-SiO_2	798	19.0	14.0	5.0	0.36	7.6

filtrate loss of the fluid. This suggests that MF0.5-SiO_2 can improve drilling fluid performance.

Considering that rocks are porous media, we use ceramic filters as filtration media to simulate formation rocks and further study the effect of MF0.5-SiO_2 on the filtration performance of ODFs. From Fig. 5(a), it can be seen that the square root of the filtration volume and time is a linear function, which is consistent with Eq. (13). The slope of the straight line is related to the permeability K of the filtering medium. The decrease in slope of the filtration loss curve means that the addition of MF-SiO_2 can reduce the permeability of ceramic filter. Moreover, the adding MF0.5-SiO_2 can reduce the filtration volume of ODF, indicating that MF0.5-SiO_2 can enhance the filtration performance of ODF. The filtration volume can indirectly reflect the quality of the filter cake. As shown in Fig. 5(b), the permeability of the original ceramic filters was 8.38 mD, while the ceramic filters without MF0.5-SiO_2 added showed a slight decrease in permeability (8.30 mD). After adding 1% MF0.5-SiO_2 nanoparticles, the permeability of ceramic filters significantly decreased (6.46 mD), indicating that the addition of MF0.5-SiO_2 can effectively reduce the permeability of ceramic filter. The filtration performance of drilling fluid is directly related to the morphology of sedimentary filter cake. In order to see the distribution of MF0.5-SiO_2 nanoparticles on the surface of ceramic filters more clearly, the surface and section of the ceramic filter was observed. The original ceramic filter has large pores, which are channels for drilling fluid filtration (Fig. S5). The MF0.5-SiO_2 nanoparticles accumulate on the surface of the filter (Fig. 5(e)) to create a dense structure, which can prevent the invasion of drilling fluid. Moreover, as shown in section (Fig. 5(f)), MF0.5-SiO_2 nanoparticles can enter the pores of ceramic filter to plugging the pores, and further minimize the invasion of drilling fluid. The above experimental results indicate that the adding MF0.5-SiO_2 nanoparticles to drilling fluid can help plug and preserve wellbore stability in addition to lowering filtration loss. After the filtration test, the images of surface of ceramic filter are displayed in Fig. 5(c), where a layer of dark brown mud cake is visible. After drying, the

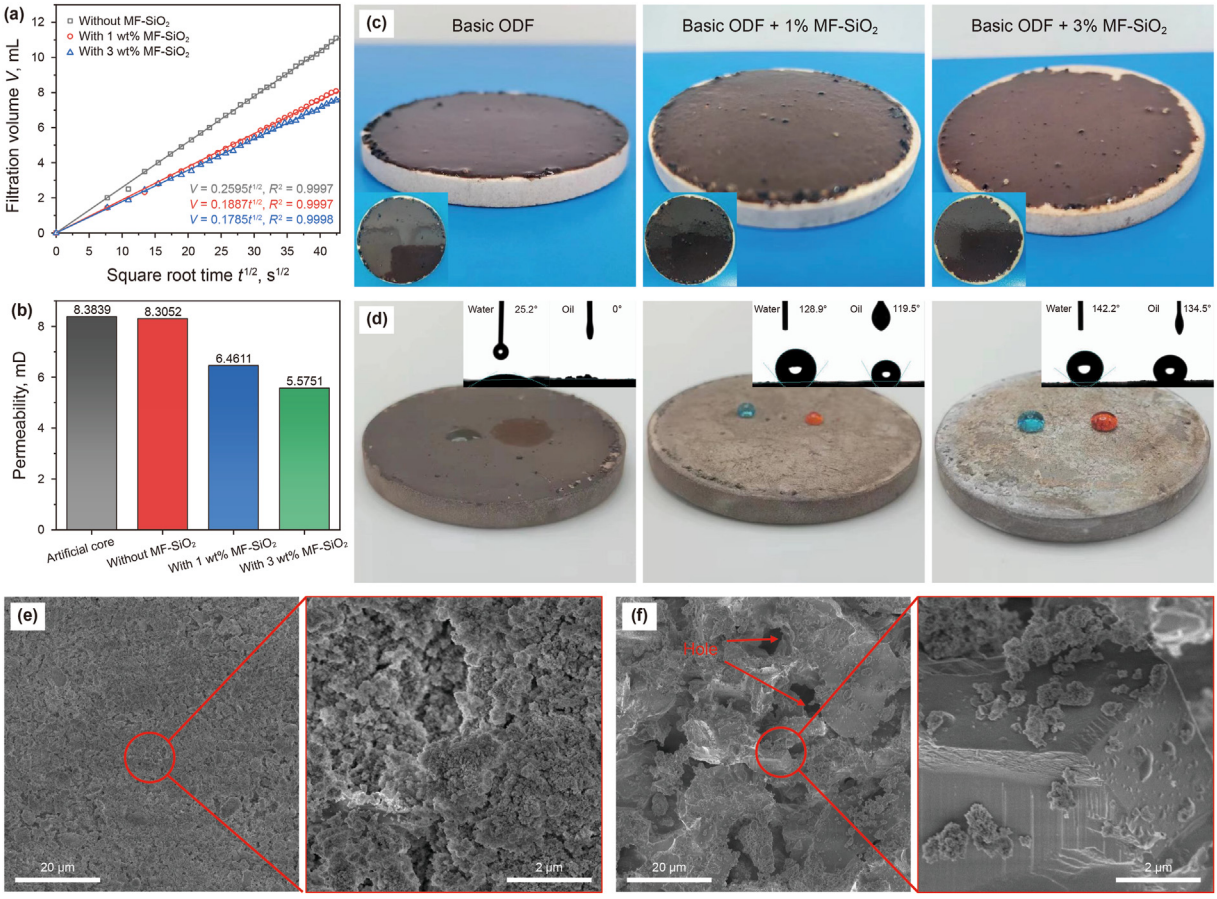

Fig. 5. (**a**) The high-temperature and high-pressure filtration volume of ODF with different concentrations of MF-SiO_2 nanoparticles as a function of the square root of time. (**b**) Permeability of original ceramic filters and MF-SiO_2 ceramic filters with different concentrations added. (**c**) Digital images of the surface of ceramic filters after filtration test. (**d**) Digital images of the spreading state of water (blue) and white oil (red) on the surface of the ceramic filter after drying. (**e**) SEM image and local enlarged image of the mud cake on the surface of the ceramic filter after filtration loss test. (**f**) SEM image and local enlarged image of the ceramic filter cross-section after filtration loss test.

contact angles between water and mineral oil on the surface of ceramic filters were measured, as shown in Fig. 5(d). For the basic ODF without adding MF-SiO_2, it is evident that water and mineral oil are spreading across the surface of mud cake. When MF-SiO_2 was introduced, mineral oil and water can maintain a good spherical shape on the surface. The contact angles of water and mineral oil are 128.9° and 119.5°, respectively. And compared to the addition of 1 wt% MF-SiO_2, the surface contact angle of the filter with 3 wt% MF-SiO_2 addition is larger. The contact angles of the water and toluene on the mud cake surfaces were measured, and the results are shown in Table S3. The surface free energy was calculated as described in Section 2.6, and the results are presented in Table S4. The surface free energy of the basic ODF was 68.81 mJ·m^{-2}. After treatment with 1 wt% MF0.5-SiO_2, the surface free energy reduced to 3.95 mJ·m^{-2}. A low level of surface free energy implies a weaker interaction force between the liquid and the mud cake. Reducing the surface free energy of the mud cake can reduce the adhesion ability of the liquid, making it easier for water, oil, or other substances to be repelled.

3.5. Maintaining the stability of shale in oil-based drilling fluids

In the method of maintaining wellbore stability, besides reducing the filtration volume of drilling fluid, altering the rock wettability seems an effective strategy. To investigate the contribution of MF-SiO_2 to wellbore stability, we soaked shale cores in ODF containing 3% MF0.5-SiO_2 for 12 h and named them as treated shale. From Fig. 6(a), it can be seen that the surface of the original shale is black, and water and mineral oil are basically in a fully spread state on the surface. There is a visible white film structure on the treated shale surface. Water, WDF, oil, and ODF can all maintain a clear spherical shape on the surfaces. Fig. S6 displays the test results for the contact angles of the shale surface both before and after treatment. On the untreated shale surface, the contact angles of water, WDF, mineral oil, and ODF were 69.3°, 79.5°, 15.8° and 9.9°, respectively. These contact angles demonstrated amphiphilic features of hydrophilicity and lipophilicity, with a greater emphasis on lipophilicity. However, after treatment, the contact angles of all four liquids significantly increased, even the contact angle of ODF exceeded 90°, indicating that adding MF0.5-SiO_2 to ODF can alter the wettability of shale. The contact angles of the water and toluene on the surfaces of shale were measured, and the results are shown in Table S5. The surface free energy of the untreated shale was 34.99 mJ·m^{-2}. After treatment with MF0.5-SiO_2, the surface free energy reduced to 8.17 mJ·m^{-2} (Table S6). The holes and fissures in shale formation allow drilling fluid to enter the rock with capillary force. The capillary force, which is proportional to the surface tension of liquids, serves as the pushing force for the liquid to enter the core pores when it is able to wet the pipe wall, according to the Laplace equation. This explains that the infiltration and absorption mass of oil and ODFs in shale is significantly lower than that of water and WDFs (Fig. 6(b) and Fig. S7). The absorption quality of the core treated with MF0.5-SiO_2 to water, mineral oil, WDF and ODF was significantly reduced. The quality and rate of infiltration are significantly reduced if the liquid is unable to wet the pipe wall since the liquid surface inside the capillary protrudes outward and

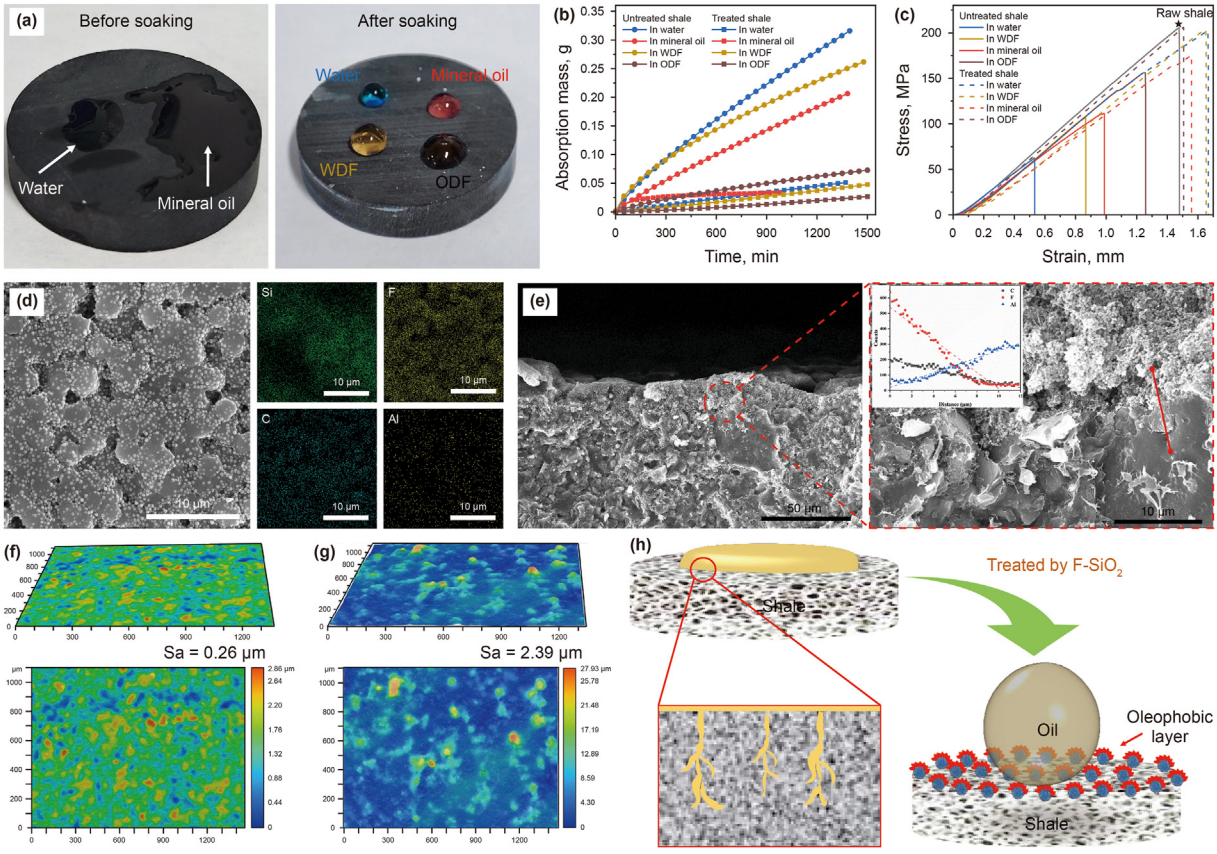

Fig. 6. (**a**) Digital images of shale surface wetting before and after soaked in ODF with 3% MF0.5-SiO_2. (**b**) Capillary imbibition experiment of shale core in water, WDF, mineral oil, and ODF. (**c**) The compressive strength of shale core immersed in water, WDF, mineral oil, and ODF. (**d**)The surface topography of shale treated by MF0.5-SiO_2 and EDS spectra of surface elements; (**e**) SEM images and locally magnified images of shale treated with MF0.5-SiO_2, the enlarged image is the element content change map of the line scan result; (**f**) The 3D morphology of original shale and (**g**) shale treated by MF0.5-SiO_2. (**h**) The mechanism of maintaining wellbore stability by MF-SiO_2.

the capillary force acts as a barrier to the entry of liquids into the core pores. The evaluation of liquid adhesion is an important parameter for the practical application of hydrophobic coatings (Chen et al., 2023). The reduced wetting force could be quantified by the adhesion force tester. As shown in Fig. S8, there are some significant differences compared with the adhesion force curves in Fig. 4(g). When the four types of droplets come into contact with the shale surface, the absolute value of adhesion force significantly increases, which is caused by the wetting force generated by the droplets wetting the surface. Moreover, due to the high adhesion force, droplets adhere to the surface of shale and cannot detach, resulting in a significant extension of the stretching process. When the droplets detach from the shale surface, the value of the force stabilizes to a negative value, which means that some of the liquid adheres to the shale surface. For shale treated with MF0.5-SiO_2 (Fig. S9), the phenomenon of an obvious increase in force caused by wetting force disappears when the droplets come into contact with the shale surface. The value of maximum adhesion force significantly decreased throughout the entire process, and the quality loss caused by the adhesion reduced significantly. These results all indicate that MF0.5-SiO_2 can significantly reduce the adhesion force of liquids on the surface of shale.

To evaluate the compressive strength of shale core, we soaked the raw shale and shale cores treated by MF0.5-SiO_2 for 28 days in water, WDF, mineral oil, and ODF. As shown in Fig. 6(c), the compressive strength of raw shale is 208.63 MPa, while the compressive strength of shale soaked in white oil and ODF without MF0.5-SiO_2 treatment is 111.39 and 156.25 MPa, respectively. Compared with the raw shale, the compressive strength has decreased by about 46.6% and 25.1%. After MF0.5-SiO_2 treatment, the compressive strength of shale decreased by approximately 16% and 2.2%, reaching 175.13 and 203.97 MPa, respectively. It can be seen that the addition of MF0.5-SiO_2 significantly slows down the decrease in shale compressive strength (Fig. S10). This is because MF-SiO_2 nanoparticles adhere to the rock surface, causing the wetting state of shale surface to change from hydrophilic and oleophilic to amphiphobic, and the capillary suction of shale pores to capillary resistance. This change in wettability can significantly reduce the invasion of drilling fluid, thereby maintaining the integrity of shale pore structure. In addition, some MF-SiO_2 nanoparticles enter the pores of shale, which can provide a certain degree of sealing effect on the pores, reduce the damage of external pressure to the pore structure, and thus improve the compressive strength of shale.

Subsequently, to investigate the mechanism of MF-SiO_2 in maintaining wellbore stability, SEM was used to observe the morphology of the shale surface and section before and after treatment. The original shale sample has a rough surface with tiny pores that drilling fluid can easily invade into (Fig. S11). After treated by MF-SiO_2, numerous spherical particles adhere to the shale surface (Fig. 6(d)). These spherical particles are MF-SiO_2, as indicated by the EDS data, which also demonstrate that the distribution of F element is extremely compatible with the distribution of these particles on the shale surface. These MF-SiO_2 nanoparticles can be uniformly adsorbed on the surface of shale. In addition, we observed the section of the shale and found that there is a sedimentary layer on the surface of the treated shale. The enlarged image of the section shows that there is a clear interface between this sedimentary layer and the shale surface. EDS was used to scan elements along the vertical line of the interface. As can be seen from the illustration in Fig. 6(e), as the scanning depth increases, the intensity of C and F elements decreases, while the intensity of Al element gradually increases. This is due to the higher content of MF-SiO_2 F and C elements in the sedimentary layer, while the silicoaluminate minerals in shale contain more Al elements. Finally, the surface roughness of original shale and treated shale were measured using a super depth of field digital microscope in a three-dimensional plane. As shown in Fig. 6(f), the surface of the original shale is generally relatively flat, with a surface roughness of 0.26 μm. After treated, sharp protrusions appeared on the surface of the shale, and the surface roughness increased to 2.39 μm (Fig. 6(g)). The surface roughness has significantly improved. According to the Wenzel's equation (Wang et al., 2022b; Deng et al., 2023),

$$\cos\theta_w = r\cos\theta \tag{15}$$

where r represents the surface roughness coefficient, which is the ratio of the actual surface area to its projected horizontal area. The contact angle of droplets is not only related to surface tension, but also to the roughness of the solid surface. The increase in surface roughness directly amplifies the wettability of the solid surface, making the hydrophobic surface more hydrophobic.

Based on the above research results, a possible mechanism was proposed for improving the wellbore stability of shale gas formations using MF-SiO_2 (Fig. 6(h)). Without the use of MF-SiO_2, the drilling fluid would invade into formation through the pores, fractures and other capillary channels under hydrostatic pressure and capillary force, which would lead to drilling fluid entering the interior of shale, reducing its mechanical strength, and even inducing serious wellbore instability accidents (Liang et al., 2017; Su et al., 2018). As a solution to the above problem, the MF-SiO_2 nanoparticles were developed that can enter and plug the interior of mud cakes and formation pores, improve the quality of mud cakes and rocks. In addition, MF-SiO_2 has the ability to absorb on the surface of rocks and mud cakes, altering their surface wettability and making it more difficult for drilling fluid to wet the shale. This also minimizes the amount of spontaneous rock infiltration caused by capillary action. Under the two effects, the MF-SiO_2 can effectively reduce the volume of fluid entering the formation in the drilling fluid, achieving the goal of stabilizing the wellbore. In addition, we have summarized the work of similar silica based wetting reversal agents (Table S7).

4. Conclusion

In this study, mesoporous SiO_2 nanoparticles featuring a wrinkled surface were prepared through a Winsor emulsion system. These nanoparticles were subsequently modified with fluorosilane to serve as an additive for oil-based drilling fluids aimed at enhancing wellbore stability in shale gas formations. The modified fluorosilane silica nanoparticles (MF-SiO_2) play a dual role in maintaining wellbore stability. First, MF-SiO_2 exhibits low surface energy, anti-adhesion properties, self-cleaning capabilities, and robust chemical and thermal stability, which enables the coating to retain its hydrophobic characteristics in environments below 200 °C. The MF-SiO_2 reduces the surface energy of the mud cake from 34.99 to 8.17 $mJ\cdot m^{-2}$ during the formation of drilling fluid mud cakes and increases the roughness of the shale surface from 0.26 to 2.39 μm, altering the wettability of rocks and reducing the liquid infiltration rate caused by capillary forces. Second, the small particle size of MF-SiO_2 allows it to penetrate the pores of the mud cakes and rocks, effectively plugging them and thereby reducing permeability. This leads to a significant decrease in the filtration volume of the drilling fluid, with the API filtration rate dropping from 11.2 to 7.6 mL. In addition, MF-SiO_2 enhances the rheological properties and emulsion stability of the drilling fluids. In summary, this work presents a novel approach to efficiently extract shale oil and gas while stabilizing wellbores in ODF applications.

CRediT authorship contribution statement

Hong-Yan Du: Writing – original draft, Supervision, Investigation, Formal analysis, Data curation, Conceptualization. **Kai-He Lv:** Funding acquisition. **Jin-Sheng Sun:** Resources, Funding acquisition. **Mei-Chun Li:** Writing – review & editing, Methodology. **Yuan Geng:** Writing – review & editing, Conceptualization. **Xian-Bin Huang:** Resources, Funding acquisition, Data curation. **Hao-Kun Shen:** Writing – original draft, Methodology, Investigation, Formal analysis, Data curation, Conceptualization. **Muhammad Arqam Khan:** Writing – review & editing.

Declaration of competing interest

The authors declare that they have no known competing financial interests or personal relationships that could have appeared to influence the work reported in this paper.

Acknowledgments

We acknowledge the financial support from the National Natural: Science Foundation of China (NO. 52174014) and the National Natural Science Foundation Basic Science Center(NO. 52288101).

Appendix A. Supplementary data

Supplementary data to this article can be found online at https://doi.org/10.1016/j.petsci.2024.12.006.

References

Ali, J.A., Hamadamin, A.B., Ahmed, S.M., Mahmood, B.S., Sajadi, S.M., Manshad, A.K., 2022. Synergistic effect of Nanoinhibitive drilling fluid on the shale swelling performance at high temperature and high pressure. Energy Fuels 36 (4), 1996–2006. https://pubs.acs.org/doi/epdf/10.1021/acs.energyfuels.1c03804.

Al-Yasiri, M., Awad, A., Pervaiz, S., Wen, D., 2019. Influence of silica nanoparticles on the functionality of water-based drilling fluids. J. Pet. Sci. Eng. 179, 504–512. https://doi.org/10.1016/j.petrol.2019.04.081.

API RP 13B-2, 2014. American Petroleum Institute Recommended Practice for Field Testing of Oil-Based Drilling Fluids.

API RP 13B-1, 2019. Recommended Practice for Field Testing Water-Based Drilling Fluids.

Assaedi, H., Shaikh, F.U., Low, I.M., 2016. Influence of mixing methods of nano silica on the microstructural and mechanical properties of flax fabric reinforced geopolymer composites. Construct. Build. Mater. 123, 541–552. https://doi.org/10.1016/j.conbuildmat.2016.07.049.

Bardhan, A., Vats, S., Prajapati, D.K., Halari, D., Sharma, S., Saxena, A., 2024. Utilization of mesoporous nano-silica as high-temperature water-based drilling fluids additive: insights into the fluid loss reduction and shale stabilization potential. Geoenergy. Sci. Eng. 232, 212436. https://doi.org/10.1016/j.geoen.2023.212436.

Basfar, S., Elkatatny, S., 2023. Micronized calcium carbonate to enhance water-based drilling fluid properties. Sci. Rep. 13 (1), 18295. https://doi.org/10.1038/s41598-023-45776-y.

Beitollahpoor, M., Farzam, M., Pesika, N.S., 2022. Determination of the sliding angle of water drops on surfaces from friction force measurements. Langmuir 38 (6), 2132–2136. https://doi.org/10.1021/acs.langmuir.1c03206.

Bellani, J., Verma, H.K., Khatri, D., Makwana, D., Shah, M., 2021. Shale gas: a step toward sustainable energy future. J. Pet. Explor. Prod. Technol. 11 (5), 2127–2141. https://doi.org/10.1007/s13202-021-01157-7.

Chen, X.X., Yin, Z.Z., Yan, J.L., Xue, M.S., Chen, Y.H., Yang, C.G., Luo, Y.D., 2023. Fabrication of ZnO@Fe_2O_3 superhydrophobic coatings with high thermal conductivity. Surf. Coat. Technol. 467, 129701. https://doi.org/10.1016/j.surfcoat.2023.129701.

Cheraghian, G., 2021. Nanoparticles in drilling fluid: a review of the state-of-the-art. J. Mater. Res. Technol. 13, 737–753. https://doi.org/10.1016/j.jmrt.2021.04.089.

Deng, S., Huang, Y.H., Hu, X.H., Wang, H., Zhao, H.J., He, J.L., 2022. Nano-Film-Forming plugging drilling fluid and bridging cross-linking plugging agent are used to strengthen wellbores in complex formations. ACS Omega 7 (26), 22804–22810. https://doi.org/10.1021/acsomega.2c02432.

Deng, Y.T., Xu, F.L., Yin, Z.Z., Xue, M.S., Chen, Y.H., He, P., Wu, J.S., Ou, J.F., Wang, F.J., Luo, Y.D., Hong, Z., 2023. Controllable fabrication of superhydrophobic alloys surface on 304 stainless steel substrate for anti-icing performance. Ceram. Int. 49 (15), 25135–25143. https://doi.org/10.1016/j.ceramint.2023.05.044.

Du, H.Y., Lv, K.H., Sun, J.S., Huang, X.B., Shen, H.K., 2022. Styrene-lauryl Eacrylate rubber nanogels as a plugging Eagent for oil-based drilling fluids with the function of improving emulsion stability. Gels 9 (1), 23. https://doi.org/10.3390/gels9010023.

Fu, Y.H., Jiang, Y.Q., Dong, D.Z., Hu, Q.H., Lei, Z.a., Peng, H., Gu, Y.F., Ma, S.G., Wang, Z.M., Yin, X.P., Wang, Z.L., 2021. Microscopic pore-fracture configuration and gas-filled mechanism of shale reservoirs in the western Chongqing area, Sichuan Basin, China. Petrol. Explor. Dev. 48 (5), 1063–1076. https://doi.org/10.1016/s1876-3804(21)60091-5.

Ganie, K., Idris, A.K., Mohshim, D.F., Sulaiman, W.R.W., Saaid, I.M., Malik, A.A., 2019. A review on the wettability alteration mechanism in condensate banking removal. J. Pet. Sci. Eng. 183, 106431. https://doi.org/10.1016/j.petrol.2019.106431.

Gao, D.W., Xie, J.J., Huang, S.M., Wu, S.Y., Wu, P.C., Huang, W.A., 2021. Research and application of evaluation methods for functional characteristics of oil-based drilling fluid in shale gas wells. Geofluids 1–9. https://doi.org/10.1155/2021/8814032.

Geng, Y., Sun, J.S., Cheng, R.C., Qu, Y.Z., Zhang, Z.L., Wang, J.H., Wang, R., Yan, Z.Y., Ren, H., Wang, J.L., 2022a. Micro/nano structured oleophobic agent improving the wellbore stability of shale gas wells. Petrol. Explor. Dev. 49 (6), 1452–1462. https://doi.org/10.1016/s1876-3804(23)60363-5.

Geng, Y., Sun, J.S., Wang, J.H., Wang, R., Yang, J., Wang, Q.B., Ni, X.X., 2021. Modified nanopolystyrene as a plugging agent for oil-based drilling fluids applied in shale formation. Energy Fuels 35 (20), 16543–16552. https://doi.org/10.1021/acs.energyfuels.1c02546.

Geng, Y., Sun, J.S., Xie, S.X., Huang, X.B., Wang, R., Wang, J.H., Wang, Q.B., 2022b. Novel use of a superhydrophobic nanosilica performing wettability alteration and plugging in water-based drilling fluids for wellbore strengthening. Energy Fuels 36 (12), 6144–6158. https://doi.org/10.1021/acs.energyfuels.2c00760.

Gholami, R., Elochukwu, H., Fakhari, N., Sarmadivaleh, M., 2018. A review on borehole instability in active shale formations: interactions, mechanisms and inhibitors. Earth Sci. Rev. 177, 2–13. https://doi.org/10.1016/j.earscirev.2017.11.002.

He, X., Chen, G.S., Wu, J.F., Liu, Y., Wu, S.a., Zhang, J., Zhang, X.T., 2023. Deep shale gas exploration and development in the southern Sichuan Basin: new progress and challenges. Nat. Gas. Ind. B. 10 (1), 32–43. https://doi.org/10.1016/j.ngib.2023.01.007.

Huang, W.J., Gao, D.L., 2022. Analysis of drilling difficulty of extended-reach wells based on drilling limit theory. Petrol. Sci. 19 (3), 1099–1109. https://doi.org/10.1016/j.petsci.2021.12.030.

Huang, X.B., Meng, X., Lv, K.H., Zhang, Z., Cao, L.H., Wang, R., Feng, J., Wu, Y.C., Sheng, W.B., 2022. Development of a high temperature resistant nano-plugging agent and the plugging performance of multi-scale micropores. Colloids Surf., A 639, 128275. https://doi.org/10.1016/j.colsurfa.2022.128275.

Huang, X.B., Sun, J.S., Lv, K.H., Liu, J.P., Shen, H.K., Zhang, F., 2018. Application of core-shell structural acrylic resin/nano-SiO_2 composite in water based drilling fluid to plug shale pores. J. Nat. Gas Sci. Eng. 55, 418–425. https://doi.org/10.1016/j.jngse.2018.05.023.

Jiang, G.C., Ni, X.X., Yang, L.L., Li, W.Q., Li, Y.Y., Deng, Z.Q., 2020. Synthesis of superamphiphobic nanofluid as a multi-functional additive in oil-based drilling fluid, especially the stabilization performance on the water/oil interface. Colloids Surf., A 588, 124385. https://doi.org/10.1016/j.colsurfa.2019.124385.

Karakosta, K., Mitropoulos, A.C., Kyzas, G.Z., 2021. A review in nanopolymers for drilling fluids applications. J. Mol. Struct. 1227, 129702. https://doi.org/10.1016/j.molstruc.2020.129702.

Katende, A., Boyou, N.V., Ismail, I., Chung, D.Z., Sagala, F., Hussein, N., Ismail, M.S., 2019. Improving the performance of oil based mud and water based mud in a high temperature hole using nanosilica nanoparticles. Colloids Surf., A 577, 645–673. https://doi.org/10.1016/j.colsurfa.2019.05.088.

Lei, Q., Xu, Y., Cai, B., Guan, B.S., Wang, X., Bi, G.Q., Li, H., Li, S., Ding, B., Fu, H.F., Tong, Z., Li, T., Zhang, H.T., 2022. Progress and prospects of horizontal well fracturing technology for shale oil and gas reservoirs. Petrol. Explor. Dev. 49 (1), 191–199. https://doi.org/10.1016/s1876-3804(22)60015-6.

Li, C.Q., Dou, P., Zhao, R.Y., Shi, Y.R., Fu, G.J., Shen, B., 2023. Preparation and superhydrophobic mechanism analysis of FAS-17-modified SiO_2/PDMS coatings for high-voltage composite insulators. Coatings 13 (3), 563. https://doi.org/10.3390/coatings13030563.

Li, H., Lv, K.H., Huang, X.B., Lu, Z., Dong, X.D., 2020a. The synthesis of polymeric nanospheres and the application as high-temperature nano-plugging agent in water based drilling fluid. Front. Chem. 8, 247. https://doi.org/10.3389/fchem.2020.00247.

Li, W.Q., Jiang, G.C., Ni, X.X., Li, Y.Y., Wang, X.Z., Luo, X.G., 2020b. Styrene butadiene resin/nano-SiO_2 composite as a water-and-oil-dispersible plugging agent for oil-based drilling fluid. Colloids Surf., A 606, 125245. https://doi.org/10.1016/j.colsurfa.2020.125245.

Li, Z.H., Yin, Z.Z., Xiao, W.B., Chen, Y.H., Yang, C.G., Luo, Y.D., Hong, Z., Xue, M.S., 2024. Facile construction of robust superhydrophobic ZIF-8@pulp/cellulose nanofiber (CNF) membrane for multifunctional applications. Ind. Crops Prod. 209, 118001. https://doi.org/10.1016/j.indcrop.2023.118001.

Liang, M.L., Wang, Z.X., Gao, L., Li, C.L., Li, H.J., 2017. Evolution of pore structure in gas shale related to structural deformation. Fuel 197, 310–319. https://doi.org/10.1016/j.fuel.2017.02.035.

Liu, K.Y., Yin, Z.Z., Luo, R.K., Qiu, B.R., Chen, Y.H., Yang, C.G., Luo, Y.D., Hong, Z., Xue, M.S., 2023. Durable $Co(OH)_2$/stearic acid-based superhydrophobic/superoleophilic nanocellulose membrane for highly efficient oil/water separation and simultaneous removal of soluble dye. Ind. Crops Prod. 203, 117190. https://

doi.org/10.1016/j.indcrop.2023.117190.
Ma, L., Luo, P.Y., He, Y., Zhang, L.Y., Fan, Y., Jiang, Z.J., 2019. Ultra-stable silica nanoparticles as nano-plugging additive for shale exploitation in harsh environments. Nanomaterials 9 (12), 1683. https://doi.org/10.3390/nano9121683.
Mao, H., Qiu, Z.S., Shen, Z.H., Huang, W.A., 2015. Hydrophobic associated polymer based silica nanoparticles composite with core–shell structure as a filtrate reducer for drilling fluid at utra-high temperature. J. Pet. Sci. Eng. 129, 1–14. https://doi.org/10.1016/j.petrol.2015.03.003.
Meng, X., Huang, X.B., Lv, K.H., Li, H., Wang, Z.Y., Wang, Z.L., Dong, X.D., Sun, J.S., Yang, Z., 2023. Core-shell structured polystyrene microspheres for improving plugging performance of oil-based drilling fluids. Colloids Surf., A 674, 131841. https://doi.org/10.1016/j.colsurfa.2023.131841.
Moon, D.S., Lee, J.K., 2012. Tunable synthesis of hierarchical mesoporous silica nanoparticles with radial wrinkle structure. Langmuir 28 (33), 12341–12347. https://doi.org/10.1021/la302145j.
Ou, X.F., Cai, J.B., Tian, J.H., Luo, B.H., Liu, M.X., 2020. Superamphiphobic surfaces with self-cleaning and antifouling properties by functionalized chitin nanocrystals. ACS Sustainable Chem. Eng. 8 (17), 6690–6699. https://doi.org/10.1021/acssuschemeng.0c00340.
Parvate, S., Dixit, P., Chattopadhyay, S., 2020. Superhydrophobic surfaces: insights from theory and experiment. J. Phys. Chem. B 124 (8), 1323–1360. https://doi.org/10.1021/acs.jpcb.9b08567.
Prajapati, D.K., Bardhan, A., Sharma, S., 2023. Microwave-assisted synthesis of zinc oxide nanoflowers for improving the rheological and filtration performance of high-temperature water-based drilling fluids. J. Dispersion Sci. Technol. 1–13. https://doi.org/10.1080/01932691.2023.2294303.
Rafieefar, A., Sharif, F., Hashemi, A., Bazargan, A.M., 2021. Rheological behavior and filtration of water-based drilling fluids containing graphene oxide: experimental measurement, mechanistic understanding, and modeling. ACS Omega 6 (44), 29905–29920. https://doi.org/10.1021/acsomega.1c04398.
Ren, D.F., Xu, J.Q., Chen, N., Ye, Z.X., Li, X.F., Chen, Q.M., Ma, S.Y., 2021. Controlled synthesis of mesoporous silica nanoparticles with tunable architectures via oil-water microemulsion assembly process. Colloids Surf., A 611, 125773. https://doi.org/10.1016/j.colsurfa.2020.125773.
Saengkaew, J., Le, D., Samart, C., Sawada, H., Nishida, M., Chanlek, N., Kongparakul, S., Kiatkamjornwong, S., 2018. Superhydrophobic coating from fluoroalkylsilane modified natural rubber encapsulated SiO_2 composites for self-driven oil/water separation. Appl. Surf. Sci. 462, 164–174. https://doi.org/10.1016/j.apsusc.2018.08.059.
Saleh, T.A., Ibrahim, M.A., 2019. Advances in functionalized Nanoparticles based drilling inhibitors for oil production. Energy Rep. 5, 1293–1304. https://doi.org/10.1016/j.egyr.2019.06.002.
Siddiqui, M.A.Q., Ali, S., Fei, H., Roshan, H., 2018. Current understanding of shale wettability: a review on contact angle measurements. Earth Sci. Rev. 181, 1–11. https://doi.org/10.1016/j.earscirev.2018.04.002.
Song, J.W., Yuan, Y., Gu, S., Yang, X.Y., Yue, Y., Cai, J.H., Jiang, G.S., 2017. 2D numerical simulation of improving wellbore stability in shale using nanoparticles based drilling fluid. Energies 10 (5), 651. https://doi.org/10.3390/en10050651.
Su, S.Y., Jiang, Z.X., Shan, X.L., Zhu, Y.F., Wang, P., Luo, X., Li, Z., Zhu, R.F., Wang, X.Y., 2018. The wettability of shale by NMR measurements and its controlling factors. J. Pet. Sci. Eng. 169, 309–316. https://doi.org/10.1016/j.petrol.2018.05.067.
Sun, J.S., Bai, Y.R., Cheng, R.C., Lv, K.H., Liu, F., Feng, J., Lei, S.F., Zhang, J., Hao, H.J., 2021. Research progress and prospect of plugging technologies for fractured formation with severe lost circulation. Petrol. Explor. Dev. 48 (3), 732–743. https://doi.org/10.1016/s1876-3804(21)60059-9.
Tahr, Z., Ali, J.A., Mohammed, A.S., 2023. Sustainable aspects behind nano-biodegradable drilling fluids: a critical review. Geoenergy Sci. Eng. 222, 211443. https://doi.org/10.1016/j.geoen.2023.211443.
Tan, Z.W., Sun, J., Wu, C.Y., Qiu, J.J., Liu, C.M., 2017. Phosphorus-containing polymers from THPS. IV: synthesis and properties of phosphorus-containing polybenzoxazines as a green route for recycling toxic phosphine (PH3) tail gas. J. Hazard Mater. 322, 540–550. https://doi.org/10.1016/j.jhazmat.2016.10.021.
Tang, X.C., Yang, H.B., Gao, Y.B., Lashari, Z.A., Cao, C.X., Kang, W.L., 2018. Preparation of a micron-size silica-reinforced polymer microsphere and evaluation of its properties as a plugging agent. Colloids Surf., A 547, 8–18. https://doi.org/10.1016/j.colsurfa.2018.03.034.
Tang, Z.Q., Tian, T.F., Molino, P.J., Skvortsov, A., Ruan, D., Ding, J., Li, Y.L., 2024. Recent advances in superhydrophobic materials development for maritime applications. Adv. Sci. 11 (16), 2308152. https://doi.org/10.1002/advs.202308152.
Wang, D.H., Jiang, Y.H., Zhu, Z.L., Yin, W.Z., Asawa, K., Choi, C.H., Drelich, J.W., 2020a. Contact line and adhesion force of droplets on concentric ring-textured hydrophobic surfaces. Langmuir 36 (10), 2622–2628. https://doi.org/10.1021/acs.langmuir.9b03953.
Wang, J.C., Gui, X.H., Li, G.S., Cao, Y.J., 2022a. Experimental study on the interaction forces between water droplets and mineral surfaces. Chem. Phys. 559, 111534. https://doi.org/10.1016/j.chemphys.2022.111534.
Wang, K., Jiang, G.C., Li, X.L., Luckham, P.F., 2020b. Study of graphene oxide to stabilize shale in water-based drilling fluids. Colloids Surf., A 606, 125457. https://doi.org/10.1016/j.colsurfa.2020.125457.
Wang, S.Q., 2018. Shale gas exploitation: status, problems and prospect. Nat. Gas. Ind. B. 5 (1), 60–74. https://doi.org/10.1016/j.ngib.2017.12.004.
Wang, X., Fu, C., Zhang, C.L., Qiu, Z.Y., Wang, B., 2022b. A comprehensive review of wetting transition mechanism on the surfaces of microstructures from theory and testing methods. Materials 15 (14), 4747. https://doi.org/10.3390/ma15144747.
Wu, P.C., Zhong, C.X., Li, Z.T., Zhang, Z., Wang, Z.Y., Huang, W.A., 2021. Oil-based drilling fluid plugging method for strengthening wellbore stability of shale gas. Geofluids 2021 (1), 6674574. https://doi.org/10.1155/2021/6674574.
Xie, Z.L., Zhu, L., Bi, S.B., Ji, H., Wang, T.Y., Huang, M.T., Zhang, H., Wu, H.M., 2023. Study on radial leakage model and law of fractured formation drilling fluid. Processes 11 (5), 1388. https://doi.org/10.3390/pr11051388.
Xu, C., Lei, C., Wang, Y., Yu, C.Z., 2022. Dendritic mesoporous nanoparticles: structure, synthesis and properties. Angew. Chem. Int. Ed. 61 (12), e202112752. https://doi.org/10.1002/anie.202112752.
Yan, X.P., Huo, B.Z., Deng, S., Kang, Y.L., He, Y., Xu, C.Y., Jing, H.R., 2024. The role of physical lost circulation materials type on the evolution of strong force chains of plugging zone in deep fractured tight reservoir. Powder Technol. 432, 119149. https://doi.org/10.1016/j.powtec.2023.119149.
Yin, Z.Z., Chen, X.X., Zhou, T.H., Xue, M.S., Li, M., Liu, K.Y., Zhou, D.P., Ou, J.F., Xie, Y., Ren, Z.M., Luo, Y.D., Hong, Z., 2022a. Mussel-inspired fabrication of superior superhydrophobic cellulose-based composite membrane for efficient oil emulsions separation, excellent anti-microbial property and simultaneous photocatalytic dye degradation. Sep. Purif. Technol. 286, 120504. https://doi.org/10.1016/j.seppur.2022.120504.
Yin, Z.Z., Cheng, Y., Deng, Y.T., Li, Z.H., Liu, K.Y., Li, M., Chen, X.X., Xue, M.S., Ou, J.F., Lei, S., Luo, Y.D., Xie, C., Hong, Z., 2022b. Functional and versatile colorful superhydrophobic nanocellulose-based membrane with high durability, high-efficiency oil/water separation and oil spill cleanup. Surf. Coat. Technol. 445, 128714. https://doi.org/10.1016/j.surfcoat.2022.128714.
Yin, Z.Z., Li, M., Li, Z.H., Deng, Y.T., Xue, M.S., Chen, Y.H., Ou, J.F., Lei, S., Luo, Y.D., Xie, C., 2023a. A harsh environment resistant robust $Co(OH)_2$@stearic acid nanocellulose-based membrane for oil-water separation and wastewater purification. J. Environ. Manag. 342, 118127. https://doi.org/10.1016/j.jenvman.2023.118127.
Yin, Z.Z., Li, Z.H., Deng, Y.T., Xue, M.S., Chen, Y.H., Ou, J.F., Xie, Y., Luo, Y.D., Xie, C., Hong, Z., 2023b. Multifunctional CeO_2-coated pulp/cellulose nanofibers (CNFs) membrane for wastewater treatment: effective oil/water separation, organic contaminants photodegradation, and anti-bioadhesion activity. Ind. Crops Prod. 197, 116672. https://doi.org/10.1016/j.indcrop.2023.116672.
Yin, Z.Z., Yuan, F., Li, M., Xue, M.S., Zhou, D.P., Chen, Y.C., Liu, X.Q., Luo, Y.D., Hong, Z., Xie, C., Ou, J.F., 2021. Self-cleaning, underwater writable, heat-insulated and photocatalytic cellulose membrane for high-efficient oil/water separation and removal of hazardous organic pollutants. Prog. Org. Coating 157, 106311. https://doi.org/10.1016/j.porgcoat.2021.106311.
Yin, Z.Z., Yuan, F., Xue, M.S., Xue, Y.H., Xie, Y., Ou, J.F., Luo, Y.D., Hong, Z., Xie, C., 2022c. A multifunctional and environmentally safe superhydrophobic membrane with superior oil/water separation, photocatalytic degradation and anti-biofouling performance. J. Colloid Interface Sci. 611, 93–104. https://doi.org/10.1016/j.jcis.2021.12.070.
You, L.J., Kang, Y.L., Chen, Z.X., Chen, Q., Yang, B., 2014. Wellbore instability in shale gas wells drilled by oil-based fluids. Int. J. Rock Mech. Min. Sci. 72, 294–299. https://doi.org/10.1016/j.ijrmms.2014.08.017.
Zha, Q.D., Chen, X.X., Wang, G.M., Chen, Y.H., Yang, C.G., Yin, Z.Z., Liu, K.Y., Luo, Y.D., Hong, Z., Xue, M.S., 2024a. A simple strategy towards construction of copper foam-based robust superhydrophobic coating based on perpendicular nanopins for long-lasting delayed icing and reduced frosting. Colloids Surf., A 690, 133798. https://doi.org/10.1016/j.colsurfa.2024.133798.
Zha, Q.D., Yao, Y.K., Yin, Z.Z., Deng, Y.T., Li, Z.H., Xie, Y., Chen, Y.H., Yang, C.G., Luo, Y.D., Xue, M.S., 2024b. Facile construction of multifunctional 3D smart MOF-based polyurethane sponges with photocatalytic ability for efficient separation of oil-in-water emulsions and co-existing organic pollutant. Chem. Eng. J. 490, 151747. https://doi.org/10.1016/j.cej.2024.151747.
Zou, C.N., Zhao, Q., Zhang, G.S., Xiong, B., 2016. Energy revolution: from a fossil energy era to a new energy era. Nat. Gas. Ind. B. 3 (1), 1–11. https://doi.org/10.1016/j.ngib.2016.02.001.